Available online at www.sciencedirect.com
SCIENCE DIRECT®
Surface and Coatings Technology 171 (2003) 11–14
SURFACE & COATINGS TECHNOLOGY
www.elsevier.com/locate/surfcoat

Initial deposition stage of $LiNb_{0.5}Ta_{0.5}O_3$ films in thermal plasma CVD

T. Yamaki[a,*], H. Yamamoto[a], S.A. Kulinich[b], K. Terashima[a]

[a]*Department of Advanced Materials Science, Graduate School of Frontier Sciences, The University of Tokyo, 5-1-5 Kashiwanoha, Kashiwa, Chiba 277-8562, Japan*
[b]*Department of Materials Engineering, Faculty of Engineering, The University of Tokyo, 7-3-1 Hongo, Bunkyo-ku, Tokyo 113-8656, Japan*

Abstract

Lithium niobate-tantalate ($LiNb_{1-x}Ta_xO_3$) epitaxial thin films have been prepared on sapphire (0 0 1) (i.e. c-plane) substrates by the thermal plasma spray chemical vapor deposition (TPS CVD) method. In order to achieve better control on the nanometer scale, it is necessary to gain detailed knowledge of the film formation mechanisms involved in film crystallinity and their relationship with the initial stage of film formation. In this work, the initial deposition stage of $LiNb_{0.5}Ta_{0.5}O_3$ films in TPS CVD was studied. The growth mode of $LiNb_{0.5}Ta_{0.5}O_3$ on sapphire (0 0 1) substrates was island growth (the Volmer–Weber mode). The islands with a triangular-pyramid-like shape formed under optimal conditions contributed to the high-crystallinity and high *c*-axis orientation of epitaxial $LiNb_{0.5}Ta_{0.5}O_3$ films. On the other hand, the nucleation of islands with a dome like shape resulted in $LiNb_{0.5}Ta_{0.5}O_3$ films with poorer both crystallinity and *c*-axis orientation. Moreover, the energy required for nucleation decreased as the liquid feed rate increased. This suggests that the deposited species might change with the liquid feed rate.

Keywords: Lithium niobate-tantalate; Initial growth; Epitaxy; Thermal plasma

1. Introduction

Lithium niobate-tantalate ($LiNb_{1-x}Ta_xO_3$), a solid solution of lithium niobate ($LiNbO_3$) and lithium tantalate ($LiTaO_3$), is a ferroelectric material with potentially good physical properties. Moreover, it is very attractive because the physical properties can be changed from those of $LiNbO_3$ at $x=0$ to those of $LiTaO_3$ at $x=1.0$. Recently, the thermal plasma spray chemical vapor deposition (TPS CVD) method has been applied by our group to the high-growth-rate deposition of $LiNb_{1-x}Ta_xO_3$ films with high-crystallinity and high *c*-axis orientation on both silicon and sapphire (0 0 1) substrates [1–3]. The influences of the substrate temperature and the liquid feed rate on film crystallinity, orientation and surface morphology have been investigated [1,2]. Yamamoto et al. [1] deposited $LiNb_{1-x}Ta_xO_3$ film on sapphire (0 0 1) substrates with the deposition rates of up to approximately 6 nm/s, which was approximately 100 times as fast as those of most conventional vapor phase deposition methods of $LiNbO_3$ or $LiTaO_3$ [4–9]. $LiNb_{1-x}Ta_xO_3$ films with $x=0.5$ exhibited a (0 0 6) rocking curve full-width at half-maximum (FWHM) value of 0.15–0.20°, which is comparable to those of $LiNbO_3$ and $LiTaO_3$ films grown by other conventional deposition techniques [4–9].

However, the initial deposition stage of $LiNb_{1-x}Ta_xO_3$ films in TPS CVD has not been investigated in detail. Thus, detailed knowledge of the mechanisms involved in the film growth and their relationship with the initial deposition stage of the film is essential. In this work, in order to achieve better control over nanostructure formation, we examined the deposition mechanism in the very early stage of film growth.

2. Experimental procedure

The outline of the TPS CVD method was described elsewhere [1,3], together with a description of the experimental setup, consisting mainly of a radio frequency (RF) plasma chamber, vacuum pumps and a liquid source feeder. For the TPS CVD method, mixtures of metalorganic solutions containing lithium–niobium and lithium–tantalum alkoxide precursors are used as liquid source materials; in this study, mixtures with Nb/Ta ratios of 1:1 were used. As-received optically polished sapphire (0 0 1) single-crystal plates ($10\times10\times0.5$

*Corresponding author. Tel.: +81-4-7136-3797; fax: +81-4-7136-3798.
E-mail address: yamaki@terra.mm.t.u-tokyo.ac.jp (T. Yamaki).

0257-8972/03/$ - see front matter © 2003 Elsevier Science B.V. All rights reserved.
doi:10.1016/S0257-8972(03)00228-7

Table 1
Typical plasma process parameters

Source Li:Nb:Ta ratio	2:1:1
Power (kW)	46.2
Pressure (Torr)	150
O_2 tangential gas flow rate (l/min)	45.0
Ar career gas flow rate (l/min)	3.0
Ar spray gas flow rate (l/min)	4.1
Ar inner gas flow rate (l/min)	5.0
Torch–substrate distance (cm)	37

mm^3 in size) were used as the substrates. In Table 1, typical plasma process parameters are listed. The initial liquid mixture was sprayed into O_2/Ar thermal plasma as a mist through an injection probe. This mist of the mixture was evaporated and completely decomposed by RF thermal plasma. Then the atoms were quenched at the boundary layer between the plasma and the substrate. Consequently, oxide film was deposited onto the substrate.

In this work, immediately after the deposition, we stopped the plasma and substrate heater in order to suppress the influence of diffusion on the substrates. After this deposition, substrate-quenching rate was estimated to be approximately 5 K/s. The deposition time was estimated from the images obtained using a digital video camera with the resolution of 1/30 s, to be 0.5 ± 0.1 s. The surface morphology of the samples was studied by high-resolution scanning electron microscopy. The microstructure was observed by transmission electron microscopy (TEM).

3. Results and discussion

In our previous work, the crystallinity of $LiNb_{0.5}Ta_{0.5}O_3$ films was studied using X-ray rocking curve measurement [1]. Fig. 1 shows the variation of the (0 0 6) rocking curve FWHM values as a function of the liquid feed rate. To elucidate this dependence, a series of $LiNb_{0.5}Ta_{0.5}O_3$ films with similar thickness of 170–190 nm was grown using different liquid feed rates. The substrate temperature was maintained at 670 ± 10 °C and the liquid feed rate was varied from 0.5 to 10 ml/min. The rocking curve FWHM decreases with increasing liquid feed rate and reaches its minimum at $R = 6$–8 ml/min. At $R > 8$ ml/min, film improvement appears to be inhibited by the contribution of a number of factors, e.g. less reliable temperature control at higher feeding rates (for comparison: ± 10 °C at $R = 8$ ml/min, whereas it was ± 5 °C at $R = 4$ ml/min) or gas phase nucleation formation of large clusters/particles at higher source material concentrations in plasma. Thus, the FWHM values could reach 0.15° at $R = 6$–8 ml/min. This result is comparable to those for $LiNbO_3$ and $LiTaO_3$ films deposited by other vapor phase deposition techniques, such as metalorganic CVD, sputtering or pulsed laser deposition [4–10].

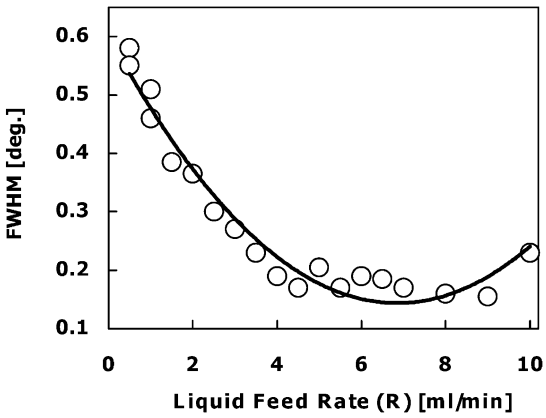

Fig. 1. Effect of liquid feed rate (R) on FWHM values of (0 0 6) rocking curves; $T_{sub} = 670 \pm 10$ °C, film thickness of 170–190 nm.

Fig. 2 shows typical SEM images. In Fig. 2a, the sample prepared at $T_{sub} = 680$ °C and $R = 4$ ml/min for 0.5 s shows many islands with a triangular-pyramid-like shape. This type of islands mainly formed under optimal conditions, in which epitaxial $LiNb_{0.5}Ta_{0.5}O_3$ films with high-crystallinity and high c-axis orientation are fabricated. On the other hand, in Fig. 2b the sample prepared at $T_{sub} = 630$ °C and $R = 6$ ml/min for 0.5 s shows many grains with a dome like shape. This type of islands

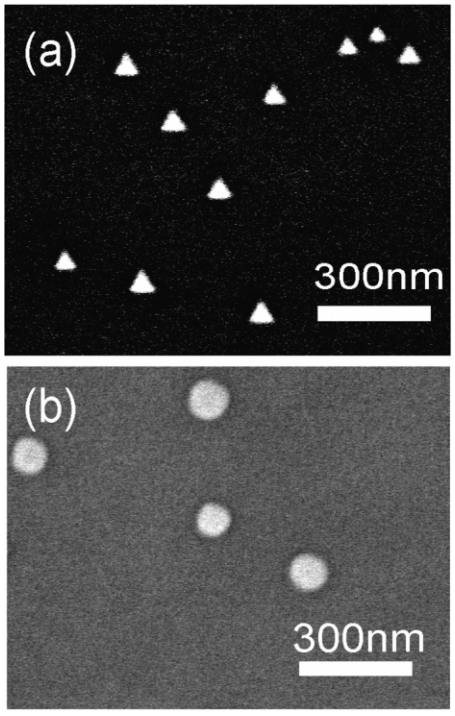

Fig. 2. SEM images of samples fabricated at (a) $R = 4$ ml/min, $T_{sub} = 680$ °C and (b) $R = 6$ ml/min, $T_{sub} = 630$ °C, respectively.

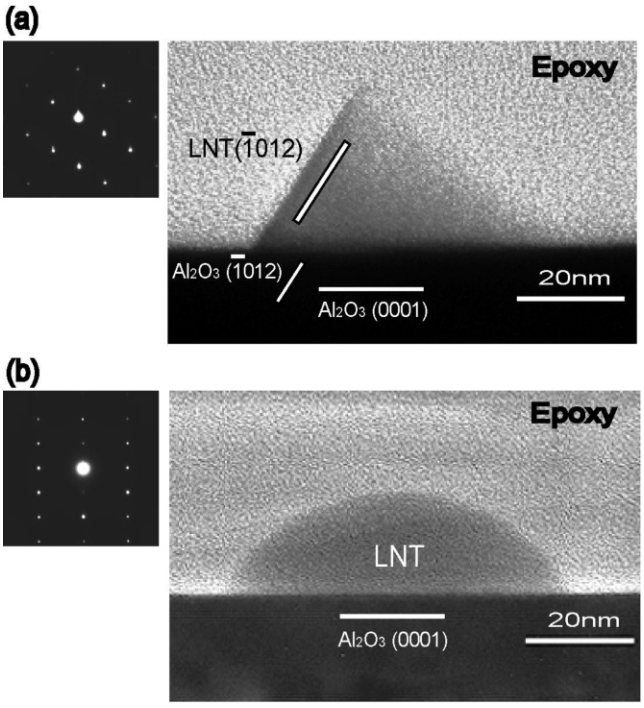

Fig. 3. Cross-sectional TEM images of samples (a) fabricated at $R=6$ ml/min, observed from the direction $[1\,\bar{2}\,1\,0]_{Al_2O_3}$ and (b) fabricated at $R=2$ ml/min, observed from the direction $[1\,0\,\bar{1}\,0]_{Al_2O_3}$, respectively.

mainly nucleated under the conditions, resulting in $LiNb_{0.5}Ta_{0.5}O_3$ films with poorer crystallinity and *c*-axis orientation.

Fig. 3a and b show typical examples of the cross-sectional TEM images of nucleation islands. Fig. 3a shows an example of an island with a triangular-pyramid-like shape. Such islands were grown epitaxially on a sapphire (0 0 1) substrate. On the other hand, Fig. 3b shows another example of an island with a dome like shape. Unlike the island in Fig. 3a, the island with the dome like shape was composed of polycrystals not epitaxially oriented to the sapphire substrate. It also consisted of a large amount of the amorphous phase. In addition, if the growth mode was Van der Merwe mode (i.e. layer by layer growth) or Stranski–Krastanov mode (i.e. layer and island growth), 1–3 layers would be deposited for 0.5 s because TPS CVD's deposition rate was approximately 6 nm/s and $LiNb_{0.5}Ta_{0.5}O_3$'s c-length was approximately 1.38 nm [11]. However, those layers were not found between the island and a sapphire (0 0 1) substrate by TEM observation.

Fig. 4 shows SEM images of samples deposited with various liquid feed rates (R, ordinate) and substrate temperatures (T_{sub}, abscissa). In these images, two types of nucleation islands, namely triangular-pyramid-like shape and dome-like shape, are observed. All the samples were prepared under the conditions of $R=4$–10 ml/min, $T_{sub}=600$–700 °C and deposition time of 0.5 ± 0.1 s. From the TEM and SEM observations, it was revealed that under these conditions the growth mode of $LiNb_{0.5}Ta_{0.5}O_3$ on sapphire (0 0 1) substrates was the island growth mode. This growth mode, which is the well-known Volmer–Weber island growth mode, is considered to be due to the large mismatch between $LiNb_{0.5}Ta_{0.5}O_3$ and sapphire (8% [10]). These two types of islands influenced the crystallinity shown in Fig. 1. Veignant et al. also reported that $LiNbO_3$ consisted of pyramidal islands in the early stage of growth when epitaxial $LiNbO_3$ was prepared on sapphire (0 0 1) substrates by pulsed laser deposition [10]. This is in good agreement with our results. The islands with a triangular-pyramid-like shape had the side length of 10–50 nm and $(\bar{1}\,0\,1\,2)$, $(1\,\bar{1}\,0\,2)$ and $(0\,1\,\bar{1}\,2)$ faces (as seen in Figs. 3 and 4). In general, the crystal face with a low crystal growth-rate often appears. Therefore, with conditions under which islands with the triangular-pyramid-like shape are formed, the growth-rate of the (0 0 0 1) face might be faster than that of another faces. As T_{sub} decreased, some triangular-pyramid-shaped islands rotated 60°. Namely, twinned grains appeared. Under this condition, film crystallinity and *c*-axis orientation became worse. As T_{sub} decreased further, the number of islands with the dome like shape became larger. Under these conditions, inferior crystal quality of the films was obtained. The islands with the dome-like shape had the radius of 10–60 nm and the height of 10–20 nm (as seen in Figs. 3 and 4).

Fig. 5 shows the relationship between the nucleation density and the inverse substrate temperature, $1000/T$. It is recognized that the nucleation density increases exponentially when the samples are prepared at lower

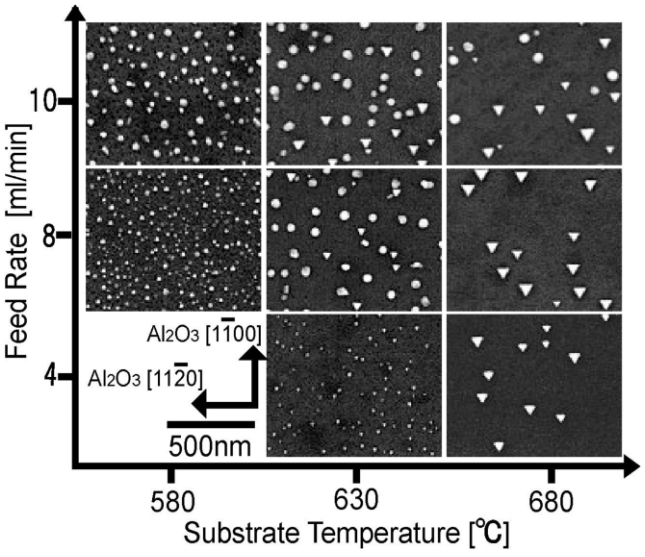

Fig. 4. SEM images of $LiNb_{0.5}Ta_{0.5}O_3$ grains grown under different temperatures and liquid feed rates.

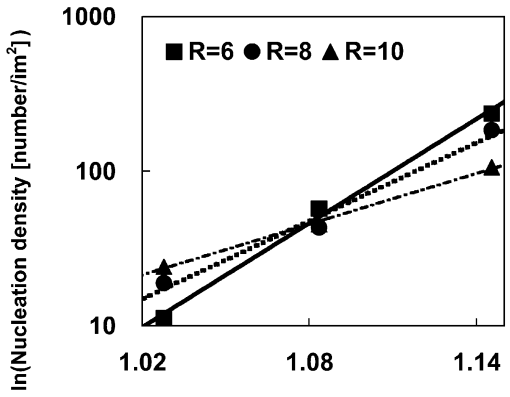

Fig. 5. Relationship between nucleation density and T_{sub}.

substrate temperatures. This tendency can be explained by referring to the well-known nucleation theory [12] described by:

$$N^* = N_o \exp(Q/kT).$$

Here, N^* is the nucleation density, N_o is the maximum possible density, Q is the energy required for nucleation, k is the Boltzmann constant, and T is the temperature. The slopes in Fig. 5 represent the energies required for nucleation.

Lee et al. [13] reported that Q was 2.57×10^{-19} J for the metalorganic CVD method. In this study, Q decreased as R increased: Q was 3.57×10^{-19}, 2.68×10^{-19} and 1.74×10^{-19} J at $R=6$, 8 and 10 ml/min, respectively. This indicates that properties of the deposited species might change with R (such as cluster size). Analogous to the plasma flash evaporation method [14], the precursor of the TPS CVD process may also be nanometer-scale clusters. This result reconfirms that the deposited species in TPS CVD might be clusters. As it was reported previously [15], nanometer-scale clusters may play important roles as the deposited species in high-crystallinity films and the high-rate deposition.

4. Conclusions

This is the first study of the initial deposition stage of $LiNb_{0.5}Ta_{0.5}O_3$ films in TPS CVD. In this work, $LiNb_{0.5}Ta_{0.5}O_3$ was deposited on sapphire (0 0 1) substrates by TPS CVD for 0.5 s. Islands with a triangular-pyramid-like shape were mainly produced under the conditions of epitaxial film growth. On the other hand, islands with a dome like shape existed under the conditions of low temperature and high liquid feed rate giving poor film crystallinity. Under these conditions, the growth mode of $LiNb_{0.5}Ta_{0.5}O_3$ on sapphire (0 0 1) substrates was the island growth mode. Moreover, the energy required for the nucleation decreased as the liquid feed rate increased. This suggests that the deposited species in TPS CVD might be clusters whose sizes change according to process parameters such as liquid feed rate.

Acknowledgments

We acknowledge Professor Toyonobu Yoshida (The University of Tokyo) for his encouragement and fruitful discussions. We also thank Junko Shibata (The University of Tokyo) for the TEM observations. The Japan Society for the Promotion of Science (JSPS) financially supported this work under the program 'Research for the Future' (97R15301).

References

[1] H. Yamamoto, S.A. Kulinich, K. Terashima, Thin Solid Films 390 (2001) 1.
[2] S.A. Kulinich, H. Yamamoto, J. Shibata, K. Terashima, T. Yoshida, Thin Solid Films 407 (2002) 60.
[3] T. Majima, H. Yamamoto, S.A. Kulinich, K. Terashima, J. Cryst. Growth 220 (2000) 336.
[4] K. Shiratsuyu, A. Sakurai, K. Tanaka, Y. Sakabe, Jpn. J. Appl. Phys. 38 (1999) 5437.
[5] H. Xie, R. Raj, Appl. Phys. Lett. 63 (1993) 3146.
[6] S.K. Park, M.S. Baek, S.C. Bae, S.Y. Kwun, K.T. Kim, K.W. Kim, Solid State Commun. 111 (1999) 347.
[7] T.N. Blanton, D.K. Chattrjee, Thin Solid Films 256 (1999) 59.
[8] Y. Shibata, K. Kaya, K. Akashi, M. Kanai, T. Kawai, J. Appl. Phys. 77 (1995) 1498.
[9] J.A. Agostinelli, G.H. Braunstein, T.N. Blanton, Appl. Phys. Lett. 63 (1993) 123.
[10] F. Veignant, M. Gandais, P. Aubert, G. Garry, Thin Solid Films 336 (1998) 163.
[11] F. Shimura, Y. Fujino, J. Cryst. Growth 38 (1977) 293.
[12] J.A. Venables (Ed.), Introduction to Surface and Thin Film Processes, Cambridge Univ. Press, Cambridge, 2000.
[13] S.Y. Lee, R.S. Feigelson, J. Cryst. Growth 186 (1998) 594.
[14] K. Terashima, K. Eguchi, T. Yoshida, K. Akashi, Appl. Phys. Lett. 52 (1988) 1274.
[15] Y. Takamura, N. Yamaguchi, K. Terashima, T. Yoshida, J. Appl. Phys. 84 (1998) 5084.